New Insights into the Fundamental Chemical Nature of Ionic Liquid Film Formation on Magnesium Alloy Surfaces

Maria Forsyth,*,† Wayne C. Neil,† Patrick C. Howlett,† Douglas R. Macfarlane,‡ Bruce R. W. Hinton,† Nathalie Rocher,† Thomas F. Kemp,§ and Mark E. Smith§

Australian Centre for Electromaterials Science, Monash University, Clayton, Victoria 3800, Australia, and Department of Physics, University of Warwick, Coventry, Warwickshire CV4 7AL, U.K.

ABSTRACT Ionic liquids (ILs) based on trihexyltetradecylphosphonium coupled with either diphenylphosphate or bis(trifluoromethanesulfonyl)amide have been shown to react with magnesium alloy surfaces, leading to the formation a surface film that can improve the corrosion resistance of the alloy. The morphology and microstructure of the magnesium surface seems critical in determining the nature of the interphase, with grain boundary phases and intermetallics within the grain, rich in zirconium and zinc, showing almost no interaction with the IL and thereby resulting in a heterogeneous surface film. This has been explained, on the basis of solid-state NMR evidence, as being due to the extremely low reactivity of the native oxide films on the intermetallics (ZrO_2 and ZnO) with the IL as compared with the magnesium-rich matrix where a magnesium hydroxide and/or carbonate inorganic surface is likely. Solid-state NMR characterization of the ZE41 alloy surface treated with the IL based on $(Tf)_2N^-$ indicates that this anion reacts to form a metal fluoride rich surface in addition to an organic component. The diphenylphosphate anion also seems to undergo an additional chemical process on the metal surface, indicating that film formation on the metal is not a simple chemical interaction between the components of the IL and the substrate but may involve electrochemical processes.

KEYWORDS: magnesium alloy • ionic liquids • surface film • NMR • corrosion

INTRODUCTION

The development of more corrosion-resistant lightweight alloys, such as those based on magnesium, is critical for the extensive use of such materials in transport and infrastructure applications. The ability to provide a protective system through the use of benign chemical treatments (compared to chromate conversion coatings) has been investigated, with sol−gel, phosphate, and modified anodizing treatments all recently reported (1−16). A novel approach to developing a barrier film has been suggested based on the interaction of an ionic liquid (IL) with the magnesium alloy surface (17−19). An IL is a low-temperature molten salt, having a melting point below 100 °C, usually composed of organic cations and anions with diffuse charges so that the Coulombic interactions are relatively weak. Typical cations are substituted quaternary ammonium, imidazolium, or phophonium salts, while anions can be, for example, Cl^-, BF_4^-, PF_6^-, and $(CF_3SO_2)_2N^-$ ($(Tf)_2N$) as well as bulkier organic anions of the carboxylate, sulfonate, and phosphonate families (20−24). In principle, the combination of cations and anions can lead to innumerable IL compounds with task-specific applications. ILs provide unique media, being composed entirely of ions. Early work has suggested that ILs based on the trihexyltetradecylphosphonium cation and coupled with organophosphate, organophosphinate, or $(CF_3SO_2)_2N^-$ anions can react with a magnesium alloy surface to produce a surface film that is more protective against corrosion than the native oxide film (17, 18).

The magnesium alloy ZE41 is an aerospace alloy typically used for helicopter gear boxes because of its high castability and excellent strength up to 160 °C. It contains zinc and rare-earth elements with zirconium added as a grain refiner, thereby creating complex phases and a heterogeneous microstructure. The low corrosion resistance of magnesium alloys, in general, is associated with these heterogeneous microstructures. Magnesium alloys are usually protected in aggressive aircraft operating environments by an anodized film (chromate containing), a primer paint (chromate containing), and top coat (25). The anodized film is necessary for good adhesion of the primer, but by itself offers very little protection (26). Several research programs (1, 11, 14, 15, 27) have concentrated on developing alternatives to the anodized film that do not contain chromate (chromates are known to be carcinogenic and toxic) and that provide some level of corrosion protection for the magnesium alloy, as well as enhance the adhesion of the paint system.

We have recently observed that certain ILs can afford some corrosion protection to ZE41 (20). An understanding of the nature of the interaction of the IL and the alloy surface, as well as the chemical nature of the resultant film, will allow a more controlled design of the process for applying ILs in order to produce uniform protective films. In this work, we

* Corresponding author. E-mail: maria.forsyth@eng.monash.edu.au.
Received for review January 10, 2009 and accepted March 12, 2009
† Department of Materials Engineering, Monash University.
‡ Department of Chemistry, Monash University.
§ University of Warwick.
DOI: 10.1021/am900023j

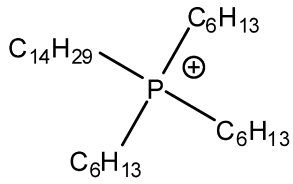

Trihexyl(tetradecyl) phosphonium ($P_{6,6,6,14}$)

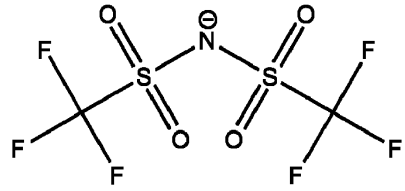

bis(trifluoromethanesulfonyl) amide $(Tf)_2N$

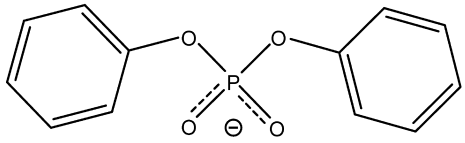

Diphenyl Phosphate (dpp)

FIGURE 1. Structures of the anion and cation of ILs.

have investigated the surface of a ZE41 alloy following immersion in an IL, based on the diphenylphosphate (dpp) or bis(trifluoromethylsulfonyl)amide ($(Tf)_2N$) anions coupled with the trihexyltetradecylphosphonium cation, using optical and electron microscopy, as well as Raman and solid-state NMR spectroscopy. Also, we have observed, using multinuclear solid-state NMR spectroscopy, the interaction of these ILs with various metal oxide/hydroxide surfaces that are expected to be part of the native oxide film formed on this alloy when it is exposed to atmospheric conditions. This approach provides new insights into the fundamental chemical interactions underlying the formation of the surface layer, which will underpin the development of these materials.

EXPERIMENTAL SECTION

Materials. The nominal composition of the ZE41 magnesium alloy investigated in this work is 3.5−5.0 zinc, 0.75−1.75 cerium (total rare earths), 0.4−1.0 zirconium, 0.15 manganese, 0.10 copper, 0.01 nickel, and 0.30 (other impurities), with the remainder magnesium (28). The $(Tf)_2N$ IL was obtained from Cytec Ltd., while the phosphate-based IL was prepared in-house, starting from Cytec Ltd. phosphonium salt, with preparative details given in ref 20.

IL Treatment. The two ILs of interest in this work are trihexyltetradecylphosphonium diphenylphosphate ($P_{6,6,6,14}$dpp, which will be referred to as "dpp") and phosphonium bis(trifluoromethanesulfonyl)amide ($P_{6,6,6,14}$ $(Tf)_2N$, which will be referred to as "$(Tf)_2N$"). The structures of these two ILs are shown in Figure 1.

IL pretreatment consisted of pouring of a few millimeter thick layer of IL onto the surface of the specimen and leaving for a set period of time. Once the treatment time had elapsed, the IL was then washed off the surface of the specimen with distilled water and ethanol and dried in a nitrogen stream.

Observation of Film Evolution Using Electrochemical Impedance Spectroscopy (EIS). EIS spectra of the surface were obtained in situ while being treated with an IL. This was achieved by using a pipet-cell arrangement, where a small area of the surface is exposed to the IL by containing the IL along with a silver wire pseudoreference electrode and platinum mesh counter electrode within a plastic pipet tip, which was clamped onto the surface of the working electrode (ZE41 surface). EIS data were acquired using an EG&G PAR VMP2/Z multichannel potentiostat with a peak-to-peak perturbation of 10 mV.

Surface Characterization. Specimens were examined using a high-power optical microscope and a JEOL 6490LA scanning electron microscope with energy-dispersive X-ray spectroscopy (EDXS). Some specimens were examined while immersed in IL using an in situ optical microscopy technique.

Optical profilometry was performed using a Veeco NT1100 optical profilometer on specimen surfaces after IL treatment.

Raman spectra were acquired using an InVia Raman spectrometer. Mounted specimens, as per the immersion tests, were used, and spectra were acquired on as-polished and IL-treated specimens. In order to obtain a reasonable Raman spectrum signal, long-time IL treatments were employed to develop a thick film on the surface. Raman mapping was employed over an area of the surface to gain an understanding of the possible different chemical environments and their relationship to the microstructure.

NMR Characterization. Powder samples of MgO lite (BDH Chemicals Ltd., 92%), Al_2O_3 (neutral surface, Aldrich), $Mg(OH)_2$ (Ventron), ZnO (BDH Chemicals Ltd., 99.7%), and ZrO_2 (Aldrich) were used as received. Samples were prepared by combining the inorganic oxide and less than 1 wt % IL using an agate mortar and pestle and vigorously mixing for 30−60 s. MgO was calcined overnight at 800 °C and cooled under nitrogen to avoid reaction of the surface. A portion of this oxide was then allowed to react with the atmosphere for 24 h before being mixed with the IL. Another fraction of this material was mixed with IL and then allowed to sit for 24 h in the rotor before acquiring the NMR data; this examines the effect of the surface reactivity of MgO. The other oxides investigated are known to be more stable in the atmosphere and hence were used only as received. Solid-state NMR was carried out with a 4-mm Bruker H-X probe under magic angle spinning (MAS) at 10 kHz on 7.05 and 8.45 T magnets, using Varian Infinity Plus and Chemagnetics Infinity consoles, respectively. Single-pulse experiments were performed for ^{19}F and ^{31}P with spectra being secondary referenced using poly(tetrafluoroethylene) (123.2 ppm, relative to $CFCl_3$) and ammonium dihydrogenphosphate (0.9 ppm relative to 85% H_3PO_4) for ^{19}F and ^{31}P, respectively.

ZE41 surfaces were immersed in the two ILs for 24 h and then dried gently using tissue paper to remove excess IL before washing thoroughly with isopropyl alcohol and further drying. The surface layers were abraded using Al_2O_3 powder and a stainless steel spatula. A dark-gray film was clearly visible on the metal surfaces, and a resultant gray powder was prepared by mixing thoroughly with the Al_2O_3 powder. The fraction of surface to powder in the sample was significantly less than 5% by volume, and hence the NMR spectra required a significant number of scans to achieve acceptable signal-to-noise ratios. In the case of the ^{31}P NMR spectra, this was obtained using a Chemagnetics Lite spectrometer operating at 82.6 MHz, and over 2×10^6 scans were accumulated. For the ^{19}F NMR spectra, an overnight run was sufficient, although the spectra were obtained after subtraction of the probe background (which was accumulated under identical conditions).

RESULTS AND DISCUSSION

dpp IL Interactions with the ZE41 Surface. The surface interaction between the IL $P_{6,6,6,14}$dpp and the alloy

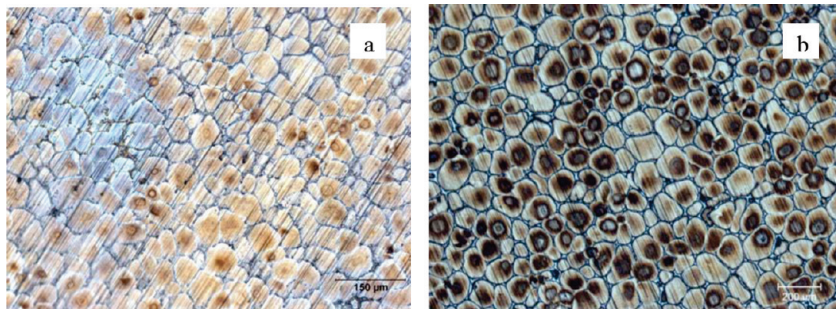

FIGURE 2. (a) ZE41 treated with dpp for 1 h; (b) ZE41 treated with dpp for 22 h.

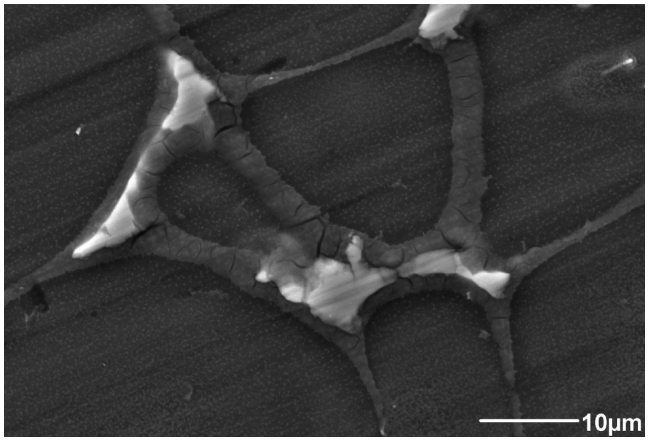

FIGURE 3. SEM image of the grain boundary region, which suggests that there is more IL interaction next to the grain boundary areas.

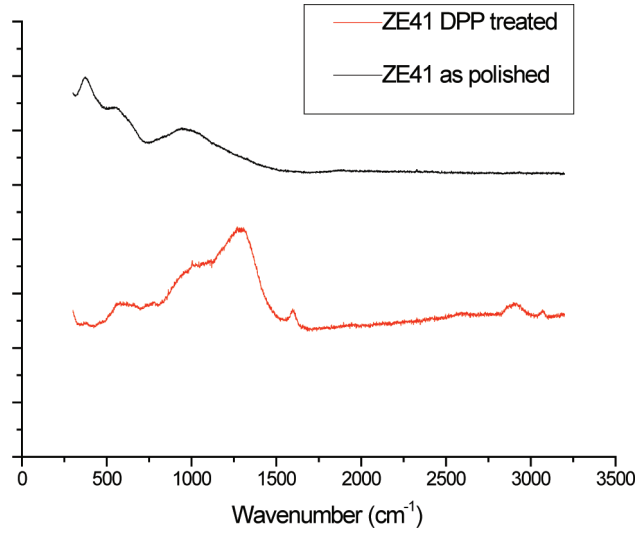

FIGURE 4. Raman spectra recorded on a pristine, as-polished ZE41 surface (top curve) and after 48 h (bottom spectrum measured away from the grain boundary). The absorbance peaks below 1000 cm^{-1} on the pristine surface represent the native surface film, with metal−oxide bonds typically seen below 500 cm^{-1}.

ZE41 can readily be visualized from optical microscopy, as shown in Figure 2. These micrographs display the immersed alloy surface after 1 and 22 h of exposure to the IL. The dark-brown coloration that begins in the center of the grains and the darkening at the grain boundaries suggest that the interaction is by no means homogeneous and also is consistent with our previous observation that corrosion is initiated at these sites (29). In other words, the center of the grains and the grain boundaries are the most reactive, the latter being directly evidenced from atomic force microscopy potential map studies of the metal surface (29). This heterogeneous reactivity has been suggested to arise from zinc-rich intermetallics that predominate at the grain boundary and zirconium-rich intermetallics at the center of the grain in this alloy (29).

The scanning electron microscopy (SEM) images for the dpp-treated surface further support that there is extensive interaction near the grain boundary; however, there is no evidence of interaction on the intermetallics themselves and, hence, the film has deposited directly adjacent to these grain boundary phases. The EDXS spectra (Figure S1 in the Supporting Information) show that the grain boundary region consists primarily of cerium, lanthanum, and zinc, with trace amounts of zirconium and little evidence of phosphorus or excessive carbon and oxygen, which would be expected if the IL was present. This therefore suggests a lack of interaction of the IL with the grain boundary phases (or, alternatively, the film is too thin to be detected). On the other hand, large O and C peaks are observed in the region neighboring the intermetallics where the thicker deposit is observed. This is consistent with a significant interaction between the magnesium-rich regions adjacent to these intermetallics. EDXS could not detect the presence of an IL-based film on the rest of the grain, and this is also most likely due to the thinness of such a film, as was previously suggested from profilometry measurements in a related alloy system (20).

Evidence of the presence of a surface film is given in Figure 4, which shows vibrational spectra obtained from Raman spectroscopy of a ZE41 surface exposed to the dpp IL for 48 h. On the bare metal, there is a broad resonance at ∼938 cm^{-1}; however, the region near 1200−1300 cm^{-1} is completely clear of any vibrations (Figure 4, top scan). In contrast to this, a ZE41 surface that is treated with the IL has a strong broad resonance centered at 1280 cm^{-1} (Figure 4, bottom scan); this is consistent with a phosphate vibration on the metal surface. If a map of the surface is taken based on this 1280 cm^{-1} resonance, then it is evident that the grain itself is mostly covered by this chemical species (Figure S2 in the Supporting Information). However, this band is missing in many regions of the grain boundary and also in the area toward the grain center, the areas previously shown to have an increase in zirconium-rich phases (29), and hence suggests that the IL cannot interact with such phases.

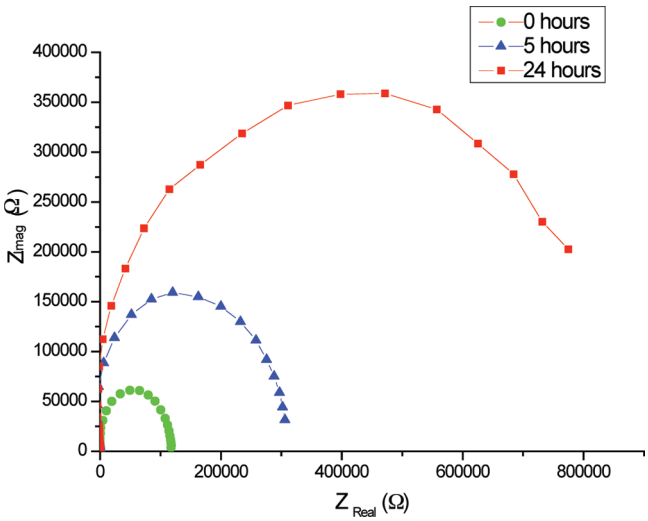

FIGURE 5. Evolution of the Nyquist plots for ZE41 in contact with the $P_{6,6,6,14}$dpp IL. The growth of the resistance can clearly be seen over a 24 h period and indicates the growth of a resistive barrier film.

Figure 5 presents an example of the in situ impedance measurements taken for the ZE41 alloy surface exposed to the dpp IL, initially and after 5 and 24 h. The obvious increase in the real axis intercept on the *x* axis, upon extrapolation of the semicircle, indicates the increase in the surface film resistivity and confirms an interaction of the IL with the metal surface. This resistivity increases by almost an order of magnitude after a 24 h exposure time. As with the SEM, the profilometry images in Figure 6 show that there is a heterogeneous interface formed after 24 h with significant thickening of the surface film around the grain boundary region. The remainder of the sample did not show an obvious appearance of the surface film indicated by the Raman spectra, but this may be due to the film being too thin to detect at this resolution.

$(Tf)_2N$ IL Interactions with the ZE41 Surface. In contrast to the dpp-based IL, the ZE41 surface does not change in appearance upon exposure to the $(Tf)_2N$-based IL, consistent with the observations made on the AZ31 surface (17, 18). In that case, only very long-term exposure led to thick deposits on the surface as observed by SEM (17, 18). The SEM for the ZE41 surface (Figure 7) is also missing any features indicative of film formation, and certainly there is no evidence of differential deposition that was observed for the dpp system (Figure 3). This suggests an alternative film formation mechanism as compared with the $P_{6,6,6,14}$dpp system. It is known that the $(Tf)_2N$ anion decomposes at reductive potentials on reactive metals such as lithium, particularly in the presence of water and/or O_2 (30), leading to the formation of LiF as well as other fluorine-containing fragments. Recent characterization of an AZ31 magnesium alloy using X-ray photoelectron spectroscopy (XPS) and time-of-flight secondary ion mass spectrometry (ToF-SIMS) after treatment in this IL also indicated the presence of F^- (31). The in situ EIS for the ZE41 coupon exposed to this IL for nearly 24 h (Figure 8) shows a rapid buildup of a resistive component on the surface, although the spectra were significantly noisy at the low-frequency end. The open-circuit potential (OCP) monitored during the film evolution showed extensive noise, indicating that an ongoing electrochemical process was likely to be occurring on the surface throughout the duration of the experiment. This is in contrast to the EIS and OCP data measured in the case of the dpp-based IL (Figure 5), where a relatively smooth steady increase in the OCP was observed and no evidence of excessive noise in the EIS spectra was detected.

Despite EIS evidence of the surface activity and film formation, there was no obvious sign of a film on the surface of the ZE41 alloy from optical microscopy or optical profilometry measurements (Figure 6). The SEM image shown in Figure 7 also lacks any clear evidence of a surface film, although our previous work with this IL and AZ31 alloy did indicate that a 24 h treatment led to a very thin film (17), which is likely to be below the detection limits of the techniques used thus far.

NMR Characterization of the IL–Substrate Interactions. There are at least three mechanisms by which the IL can interact with the metallic surface: (i) the anion can adsorb onto the metal (or metal oxide) surface followed by an electrostatic interaction with the cation to ensure charge neutrality, thereby forming a double layer on the substrate; (ii) the anion chemically interacts with the metal ions (e.g., Mg^{2+}) that may form because of surface corrosion in the immersion environment; (iii) the anion (and/or cation) electrochemically breaks down to form new chemical species, which can then interact with the surface via chemical adsorption or by the formation of insoluble surface films with Mg^{2+} or other metal ion species. The third process would be a reductive process because the metals of interest here are highly electronegative (pure magnesium has an E_0 less than −2.7 V vs SHE).

If the adsorption mechanism dominates, then the interaction is likely to be primarily via the native oxide or hydroxide that always exists on a given metal surface. Therefore, a simple examination of the reactivity of an IL with typical oxide/hydroxide compounds may give us some indication of the likelihood of this type of film formation on the metal substrate. We have previously shown that multinuclear solid-state NMR spectroscopy can elucidate such interactions (32), and hence this method was used here to determine whether the different phases in the ZE41 alloy have different characteristics with respect to IL adsorption.

Figure 9 presents the ^{31}P NMR spectra for the dpp- and $(Tf)_2N$-based ILs that have been adsorbed onto Al_2O_3, MgO, ZrO_2, and $Mg(OH)_2$ powders. The ^{31}P NMR data show two resonances attributed to the phosphonium cation (32 ppm) and the dpp anion (−11 ppm) and indicate that the cation is principally unaffected by the presence of the inorganic surface. On the other hand, the anion resonance is somewhat broadened in the case of the $Mg(OH)_2$ surface compared to the ^{31}P NMR resonance for the cation. This is consistent with our previous observations for the SiO_2 surface, also known to be well-hydroxylated (32), and confirms that these anions can strongly adsorb onto such surfaces. What is more surprising is the contrast between

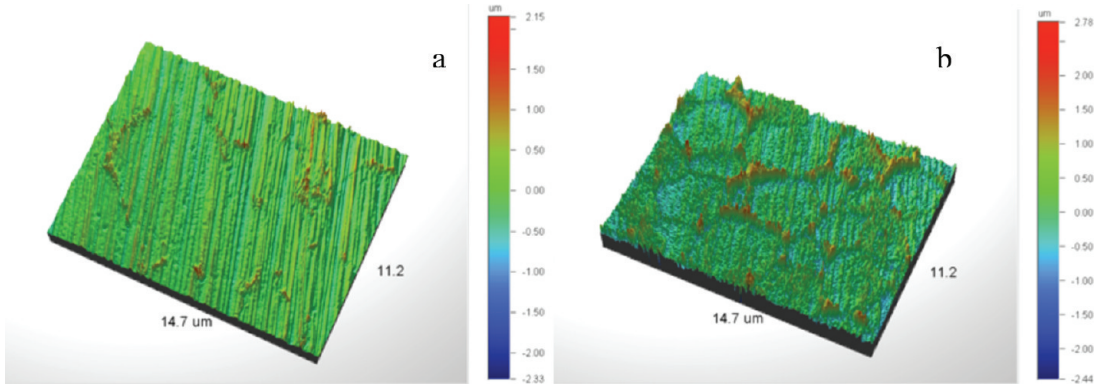

FIGURE 6. Surface of (a) an untreated and (b) a dpp-treated surface of ZE41. The interaction near the grain boundaries and the heterogeneity of the interaction with the IL are clearly seen here.

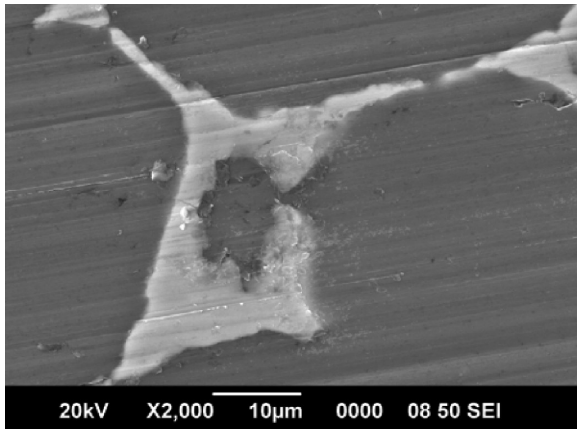

FIGURE 7. SEM image of a $P_{6,6,6,14}(Tf)_2N$-treated ZE41 surface after 24 h of treatment at room temperature.

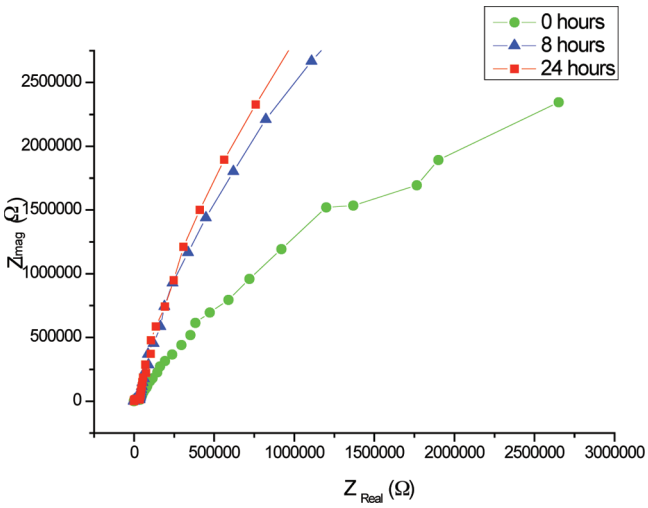

FIGURE 8. Evolution of the Nyquist plots for ZE41 in contact with the $P_{6,6,6,14}(Tf)_2N$ IL. The growth of the resistance can only be inferred here because the impedances are so large that they exceed the instrument capability. A second smaller arc is also present with a real-axis touchdown of approximately 40 000 Ω.

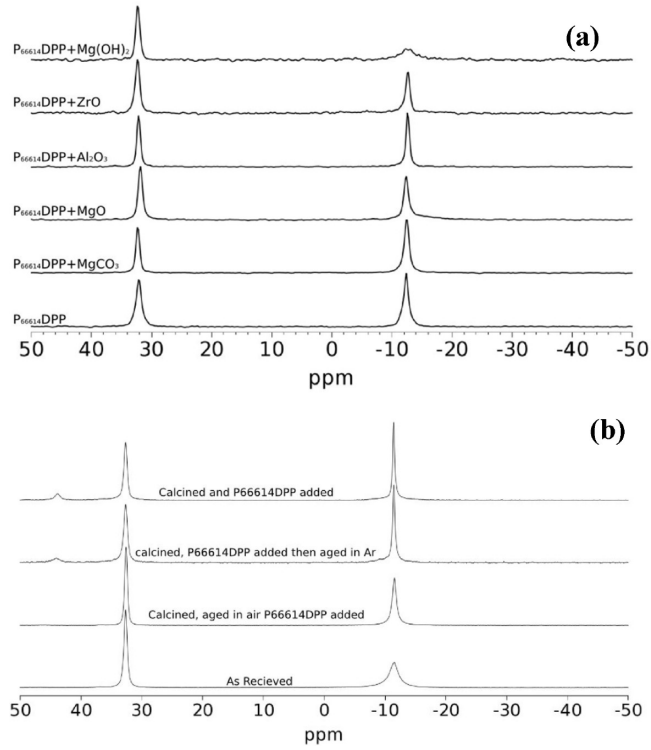

FIGURE 9. ^{31}P NMR spectra for (a) $P_{6,6,6,14}$dpp pure and adsorbed onto inorganic powders, indicating that the resonance at −32 ppm (associated with the cation) is little altered in all cases while that at −11 ppm broadens significantly in the case of $Mg(OH)_2$, and (b) $P_{6,6,6,14}$dpp adsorbed onto MgO surfaces, as received and following calcining and various exposures.

$Mg(OH)_2$ and the as-received MgO (seen in Figure 9b) surface and the other oxides that might be expected to be present in some related form on the alloy surface, in particular, at the ZE41 grain boundary and intermetallic regions that are rich in zirconium and zinc. These data suggest that a ZE41 alloy, having been exposed to atmospheric conditions and thus covered with oxidation product, will only interact strongly with the $P_{6,6,6,14}$dpp IL if it contains hydroxide groups. Because ZrO_2 are stable oxides, they are less likely to hydrolyze on the surface and thus will not readily interact with the dpp anion. This is entirely consistent with the observations made above in both optical and SEM measurements. On the other hand, the oxide that forms on the magnesium-rich matrix will react rapidly with water and CO_2 in the atmosphere and quickly become a mixture of $Mg(OH)_2$ and/or $MgCO_3$; this is indicated by the spectra in Figure 9b, where the anion resonance is broadened in the "as-received" MgO and the MgO that has been calcined to remove all of the hydroxide and carbonate groups and then subsequently allowed to react with the atmosphere for 24 h prior to adding the $P_{6,6,6,14}$dpp IL. This may account for the heterogeneity

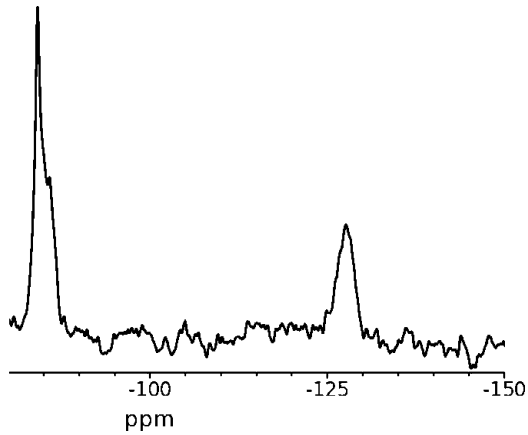

FIGURE 10. ^{19}F MAS spectrum collected at 10 kHz on a 7 T magnet. The sample was removed from the surface of a ZE41 alloy that had been immersed in IL, based on the $(Tf)_2N$ anion, for 24 h.

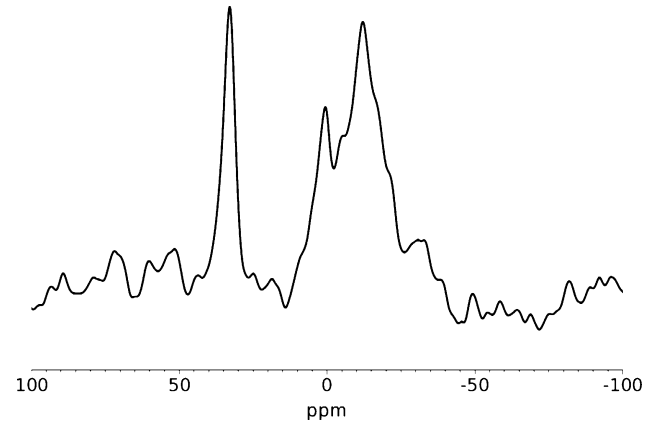

FIGURE 11. ^{31}P MAS NMR spectrum collected at 82.6 MHz, spinning at 10 kHz on a 4.79 T magnet. The sample was removed from the surface of a ZE41 alloy that had been immersed in IL, based on the DPP anion, for 24 h.

observed on the ZE41 surface and may also indicate a possible route to achieving an improved IL surface film on a magnesium alloy by preactivating the surface with OH^-.

The ^{19}F NMR data (Figure S3 in the Supporting Information) indicated a less dramatic effect in the $(Tf)_2N^-$ anion spectrum, with only subtle changes being observed. This was surprisingly in contrast to the spectra observed for the same IL adsorbed onto SiO_2, where very significant interaction with this anion is clear (32). The other interesting observation from this NMR data is that there is no evidence of chemical breakdown or hydrolysis of the species in these ILs, which removes the possibility that the phosphonium cation may form P—O—M (where M is the metal ion in the oxide or hydroxide) bonds on the surface of oxides.

Again the NMR observations are consistent with the optical and SEM images, which do not indicate any strong preferential interaction between the $(Tf)_2N$-based IL and the ZE41 surface.

If the electrochemical decomposition mechanism was dominant on this substrate, as has been previously suggested for surface films on lithium metal (30), then the NMR characterization of the interphase region, after its mechanical removal from the metal substrate, would show chemical species different from those in the pure IL. Figures 10 and 11 show the MAS NMR spectrum for ^{31}P from the surface film removed after 24 h of immersion in a ZE41 coupon in the dpp IL and the ^{19}F MAS NMR spectrum after a similar immersion time in the $(Tf)_2N$ IL, indicating the different chemical species present.

The spectra shown here are quite noisy (despite long acquisition times) because of the small filling factor in the 4-mm rotor. The ^{31}P NMR data show that both the cation and anion are present on the ZE41 surface, although the anion is significantly broadened. This confirms that the chemical adsorption on the metal surface is the dominant process with this IL. However, a further peak is also seen at approximately 8 ppm, which may be attributed to a change in the environment for the phosphate group. This could occur either via a reduction of some of the phosphate anions or from a hydrolysis reaction on the OH-containing surface. The latter is indicated schematically in Figure 12.

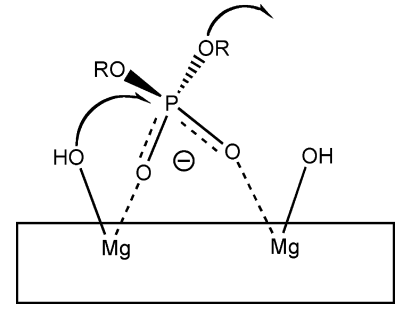

FIGURE 12. Schematic indicating the possible surface interaction of the dpp anion with the hydroxy-covered magnesium surface.

Scheme 1

$$[(PhO)_3PO] + e^- \rightarrow [(PhO)_3PO]^{-\bullet} \rightarrow Ph\bullet + [(PhO)_2PO_2]^-$$

$$[(PhO)_2PO_2]^- + e^- \rightarrow [(PhO)_2PO_2]^{2-\bullet} \rightarrow Ph\bullet + [(PhO)PO_3]^{2-}$$

In the case of electrochemical reduction of the dpp anion prior to any film formation, it has been shown (33, 34) that the triphenylphosphate species undergoes reduction, as shown in Scheme 1, where the phosphate environment itself is maintained but the phenyl group is cleaved. One could envisage that the diphenyl derivative would undergo a similar reaction and thus the local phosphorus environment would be only slightly altered, thereby leading to a slight shift in the phosphate resonance as observed on the surface product from the ZE41 treated with the dpp-based IL. This could lead to metal ester formation, as shown in Figure 12 discussed above.

In the case of the ^{19}F NMR spectrum, significant differences are seen compared to the pure IL or the IL adsorbed onto the oxide surfaces. A broad peak at −120 ppm reflects a breakdown of the $(Tf)_2N$ anion to smaller units. This may be SO_3CF_2, CF_2, or even F^- species. The latter may form metal fluorides that then deposit onto the metal surface, e.g., MgF_x, ZnF_x, or ZrF_x species, all of which, in the pure crystalline state, have resonances significantly more negative than that observed here; however, as discussed by Miller (35), their defective structures will shift the resonances.

These species are likely to form from the reduction processes of the $(NTf)_2$ anion, which has been shown to

Scheme 2[a]

$$N(SO_2CF_3)_2^- + e^- \rightarrow NSO_2CF_3^- + SO_2CF_3^-$$

$$R\text{-}CF_3 + \text{reactive Li metal surface} \rightarrow R\text{-}CF_2Li + LiF$$

[a] Adapted from Aurbach (36).

react at potentials below −2 V. The suggested pathway involves the reduction of the anion (Scheme 2) to form a new anion, $SO_2CF_3^-$, and a reactive radical species, $^{\bullet}NSO_2CF_3^-$, which can further break down to form the CF_2- or F^--containing species clearly detected on the ZE41 surface. These types of breakdown products have also been suggested by Aurbach et al. (36) and Howlett et al. (37) on reactive lithium metal surfaces where RCF_2Li and LiF were also detected.

These electrochemical reactions could also readily occur on a magnesium alloy surface given that the E_0 value of magnesium is −2.7 V (vs SHE), and therefore the combination of products that form on the surface is more complex than what would be expected for the dpp anion. Further surface characterization work (including ToF-SIMS and XPS) is needed to clarify the nature and homogeneity of the film formed in the case of the $(Tf)_2N$-based IL (although recent work based on the AZ31 alloy does suggest that a thin F^--based film is indeed present (31, 38).

CONCLUSIONS

The reactivity of two phosphonium cation based ILs with a ZE41 magnesium aerospace alloy was investigated using a combination of microscopy, electrochemical, and spectroscopic techniques. The microscopy and Raman spectroscopy clearly indicated the heterogeneous nature of the interaction of the IL based on the dpp anion, with a buildup of the surface film evident on the regions adjacent to the grain boundaries where intermetallic particles are predominantly found. In contrast, the IL based on the bis(trifluoromethanesulfonyl)-amide anion did not produce an interphase that was obviously evident on the metal surface, although the evolution of the EIS spectra strongly suggested that a film did indeed form. The presence of a surface film was confirmed by the ^{19}F and ^{31}P solid-state MAS NMR spectra obtained from the treated ZE41 surface. This fundamental study of the IL−alloy interactions suggested that the nature of the oxide present on a heterogeneous alloy is likely to lead to heterogeneous film formation when an organophosphate-based IL is used and that the film deposition is not simple physisorption of the anion on the oxide surface but is likely to involve a chemical or electrochemical process. This will impact the further design of IL systems for application in tribology and corrosion engineering where the interphase that develops on the metal alloy surface is critical in extending the lifetime of metal-based structures.

Acknowledgment. This work was enabled via an EPSRC international fellowship and the Australian Research Council, through the Australian Centre for Electromaterials Science. W.C.N. was also funded through an Australian Postgraduate Award. The authors gratefully acknowledge this support. D.R.M. is grateful to the ARC for a Federation Fellowship.

Supporting Information Available: Figures showing the EDXS analysis associated with the electron micrograph of Figure 2, the Raman map associated with spectra of Figure 4, and ^{19}F NMR data for the IL adsorbed onto inorganic oxides. This material is available free of charge via the Internet at http://pubs.acs.org.

REFERENCES AND NOTES

(1) Saijo, A.; Murakami, K.; Hino, M.; Kanadani, T. *Mater. Trans.* **2008**, *49*, 903–908.
(2) Zhao, M.; Wu, S. S.; Luo, J. R.; Fukuda, Y.; Nakae, H. *Surf. Coat. Technol.* **2006**, *200*, 5407–5412.
(3) Kouisni, L.; Azzi, M.; Zertoubi, M.; Dalard, F.; Maximovitch, S. *Surf. Coat. Technol.* **2004**, *185*, 58–67.
(4) Lin, C. S.; Lee, C. Y.; Li, W. C.; Chen, Y. S.; Fang, G. N. *J. Electrochem. Soc.* **2006**, *153*, B90−B96.
(5) Kouisni, L.; Azzi, M.; Dalard, F.; Maximovitch, S. *Surf. Coat. Technol.* **2005**, *192*, 239–246.
(6) Zucchi, F.; Frignani, A.; Grassi, V.; Trabanelli, G.; Monticelli, C. *Corros. Sci.* **2007**, *49*, 4542–4552.
(7) Supplit, R.; Koch, T.; Schubert, U. *Corros. Sci.* **2007**, *49*, 3015–3023.
(8) Khramov, A. N.; Balbyshev, V. N.; Kasten, L. S.; Mantz, R. A. *Thin Solid Films* **2006**, *514*, 174–181.
(9) Lamaka, S. V.; Montemor, M. F.; Galio, A. F.; Zheludkevich, M. L.; Trindade, C.; Dick, L. F.; Ferreira, M. G. S. *Electrochim. Acta* **2008**, *53*, 4773–4783.
(10) Hsiao, H. Y.; Tsai, W. T. *Surf. Coat. Technol.* **2005**, *190*, 299–308.
(11) Hsiao, H. Y.; Tsung, H. C.; Tsai, W. T. *Surf. Coat. Technol.* **2005**, *199*, 127–134.
(12) Shi, Z. M.; Song, G. L.; Atrens, A. *Corros. Sci.* **2005**, *47*, 2760–2777.
(13) Shi, Z. M.; Song, G. L.; Atrens, A. *Corros. Sci.* **2006**, *48*, 3531–3546.
(14) Zhang, Y. J.; Yan, C. W.; Wang, F. H.; Lou, H. Y.; Cao, C. N. *Surf. Coat. Technol.* **2002**, *161*, 36–43.
(15) Hoche, H.; Scheerer, H.; Probst, D.; Broszeit, E.; Berger, C. *Surf. Coat. Technol.* **2003**, *174*, 1002–1007.
(16) McAdam, G.; Talevski, J.; Trueman, A. R.; Danek, S.; Hinton, B. R. W. *Corros. Mater.* **2005**, *30*, 13–20.
(17) Forsyth, M.; Howlett, P. C.; Tan, S. K.; MacFarlane, D. R.; Birbilis, N. *Electrochem. Solid-State Lett.* **2006**, *9*, B52−B55.
(18) Birbilis, N.; Howlett, P. C.; MacFarlane, D. R.; Forsyth, M. *Surf. Coat. Technol.* **2007**, *201*, 4496–4504.
(19) Howlett, P. C.; Zhang, S.; MacFarlane, D. R.; Forsyth, M. *Aust. J. Chem.* **2007**.
(20) Sun, J.; Howlett, P. C.; MacFarlane, D. R.; Lin, J.; Forsyth, M. *Electrochim. Acta* **2008**, *54*, 254–260.
(21) Macfarlane, D. R.; Forsyth, M.; Howlett, P. C.; Pringle, J. M.; Sun, J.; Annat, G.; Neil, W.; Izgorodina, E. I. *Acc. Chem. Res.* **2007**, *40*, 1165–1173.
(22) Sun, J.; MacFarlane, D. R.; Forsyth, M. *Electrochim. Acta* **2003**, *48*, 1707–1711.
(23) Golding, J.; Forsyth, S.; MacFarlane, D. R.; Forsyth, M.; Deacon, G. B. *Green Chem.* **2002**, *4*, 223–229.
(24) Sun, J.; Forsyth, M.; Macfarlane, D. R. *J. Phys. Chem. B* **1998**, *102*, 8858–8864.
(25) Gray, J. E.; Luan, B. *J. Alloys Compd.* **2002**, *336*, 88–113.
(26) http://www.magnesium-elektron.com/about-magnesium.asp?ID=2, Magnesium Elektron, 2007.
(27) Zhao, Q.; Zhou, Y.; Zhang, Y.; Zhao, C.; Guo, Y.; Cang, X. *Magnesium Technol.* **2005**, 481–484.
(28) Aerospace Material Specification AMS4439E, Magnesium Alloy Castings 4.2Zn−1.2Ce−0.7Zr (ZE41A-T5) Precipiation Heat Treated, 2001.
(29) Neil, W. C.; Forsyth, M.; Howlett, P. C.; Hutchinson, C. R.; Hinton, B. R. W. *Corros. Sci.* **2009**, *51*, 387–394.
(30) Howlett, P. C.; Izgorodina, E. I.; Forsyth, M.; MacFarlane, D. R. *Z. Phys. Chem. (Muenchen, Ger.)* **2006**, *220*, 1483–1498.
(31) Howlett, P. C.; Tan, S. K.; Zhang, S.; Efthimiadis, J.; MacFarlane, D. R.; Forsyth, M. Corrosion and Protection. Australasian Corrosion Association Conference, Hobart, Australia, 2006.
(32) Forsyth, M.; Kemp, T. F.; Howlett, P. C.; Sun, J.; Smith, M. E. *J. Phys. Chem. C* **2008**, *112*, 13801–13804.

(33) Yanilkin, V. V.; Budnikova, Y. G.; Kargin, Y. M.; Gritsenko, E. I.; Strelets, V. V. *Russ. Chem. Bull.* **1990**, *39*, 1149–1152.
(34) Johnson, D. W.; Morrow, S.; Forster, N. H.; Saba, C. S. *Chem. Mater.* **2002**, *14*, 3767–3775.
(35) Miller, J. M. *Prog. Nucl. Magn. Reson. Spectrosc.* **1996**, *28*, 255–281.
(36) Aurbach, D.; Weissman, I.; Zaban, A.; Chusid, O. *Electrochim. Acta* **1994**, *39*, 51–71.
(37) Howlett, P. C.; Brack, N.; Hollenkamp, A. F.; Forsyth, M.; MacFarlane, D. R. *J. Electrochem. Soc.* **2006**, *153*, A595—A606.
(38) Howlett, P. C.; et al. To be published.

AM900023J